

MACRO-LLM: LLM-Empowered Multi-Agent Collaborative Reasoning under Spatiotemporal Partial Observability

Handi Chen, Running Zhao*, Xizhe Wu*, Edith C.H. Ngai†,

The University of Hong Kong,

{hdchen, rnzhao}@connect.hku.hk {xzwu, chngai}@eee.hku.hk

Abstract

Large Language Model (LLM) agents deployed in complex real-world scenarios typically operate as spatially distributed entities. However, this physical dispersion constrains agents to limited local perception and finite temporal horizons. We characterize this bottleneck as *spatiotemporal partial observability*. Given such fragmented awareness, distributed agents struggle to coordinate efficiently. To bridge this gap, we introduce **MACRO-LLM**, LLM-empowered multi-agent collaborative reasoning under spatiotemporal partial observability. The architecture addresses spatiotemporal constraints via three modules: (1) the CoProposer mitigates *temporal uncertainty* by verifying candidate actions via predictive rollouts; (2) the Negotiator overcomes *spatial myopia* by resolving conflicts through mean-field statistical aggregation; and (3) the Introspector ensures continuous adaptation by analyzing historical experience to refine strategies via semantic gradient descent. Extensive evaluations on two complex long-horizon tasks, cooperative adaptive cruise control and pandemic control, demonstrate that our framework effectively mitigates spatiotemporal partial observability through spatial and temporal strategies, enabling robust coordination.

1 Introduction

Large Language Model (LLM) agents have demonstrated remarkable human-like capabilities in problem-solving (Zhu et al., 2023; Cui et al., 2025). While these agents successfully automate tasks across domains such as healthcare (Wang et al., 2025; Khasentino et al., 2025) and education (Zhao et al., 2025; Shi et al., 2025), single agents often struggle with complexity and scalability in long-horizon scenarios. Consequently, inspired

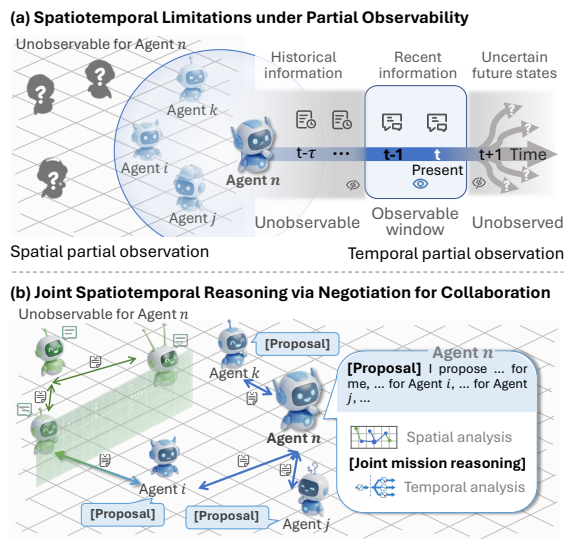


Figure 1: Illustration of spatiotemporal partial observability and the proposed collaborative reasoning framework. (a) Agents are constrained by limited local perception (spatial) and future uncertainty coupled with finite context windows (temporal). (b) Agents mitigate these limitations by exchanging proposals to establish collaborative framework via neighborhood negotiation.

by the team collaboration in human societies, researchers are actively exploring systems where multiple LLM agents cooperate toward common objectives (Li et al., 2023a; Wang et al., 2024). This collective intelligence amplifies individual capabilities, enabling the effective resolution of complex reasoning tasks through coordination and negotiation (Zou et al., 2025).

However, a critical challenge emerges when deploying these systems in complex real-world scenarios (Chen et al., 2025). Unlike centralized environments, agents in the physical world operate as distributed entities, which inherently impose spatiotemporal partial observability. Specifically, physical dispersion constrains agents to limited local perception, while the LLM's fixed context window restricts their historical temporal informa-

*Equal contribution

†Corresponding author

tion. For example, in autonomous driving, vehicles are bound by communication limits and privacy constraints, forcing them to optimize traffic flow using only local data. Therefore, addressing the partial observability stemming from real-world distribution is pivotal for enhancing collaborative efficiency and effectiveness.

Specifically, partial observability manifests along two dimensions: *spatial* and *temporal*, as illustrated in Fig. 1(a). *Spatially*, constrained by communication limits and environmental complexity, each agent perceives only a fraction of the global state, preventing it from inferring the full context of the collective task. *Temporally*, agents face inherent uncertainty regarding future dynamics. Due to the stochastic nature of the environment and the unpredictable behaviors of others, the long-term consequences of current actions are difficult to predict. This forward-looking ambiguity, compounded by finite historical context, makes it challenging to align short-term decisions with long-term global objectives. Consequently, agents operate with a patchwork of incomplete spatial information and limited temporal understanding, resulting in suboptimal, inconsistent, or even conflicting actions that significantly degrade collective efficiency and effectiveness.

Existing LLM-based Multi-Agent Systems (MAS) aim to expand their spatial perception through inter-agent communication, as shown in Fig. 1 (b). This is typically implemented via hierarchical structures that aggregate information to a central node (Yu et al., 2024; Estornell et al., 2025) or fully-connected graphs that construct a pseudo-global view (Chan et al., 2023). However, these methods often incur severe communication bottlenecks at central nodes or prohibitive overheads, limiting their scalability in large-scale, dynamically evolving environments. From a temporal perspective, while equipping agents with memory modules helps mitigate limited historical observations (Park et al., 2023; Zhang et al., 2024), the inherent unpredictability of future states remains a critical challenge. This uncertainty makes it difficult for agents to align immediate actions with long-term goals and capture cascading temporal effects. Prior to the rise of LLM-based MAS, Multi-Agent Reinforcement Learning (MARL) provides a traditional framework for addressing partial observability. Nonetheless, MARL algorithms typically suffer from poor generalization and excessive training costs (Huh and Mohapatra, 2023). As illus-

trated in Fig. 7 for pandemic control tasks, training MARL models is computationally expensive. Such inflexibility and high resource demands severely restrict the feasibility of MARL solutions for complex real-world applications.

In this paper, we propose MACRO-LLM, an LLM-empowered multi-agent collaborative reasoning under spatiotemporal partial observability, for efficient collaboration that can be generalized across diverse domains. To address spatial constraints, MACRO-LLM employs a neighborhood negotiation mechanism that combines iteratively refined semantic strategies with statistical spatial features, enabling a global understanding and coordinated decisions. To enhance temporal reasoning, MACRO-LLM integrates long-term future planning and short-term verification, continually updating strategies based on historical negotiation data. Specifically, each agent consists of three core modules: (1) the CoProposer, which generates collaborative action proposals and validates their feasibility via predictive rollouts to simulate short-term future states; (2) the Negotiator, which resolves conflicting proposals by analyzing both semantic strategies and mean-field statistical estimations of unobservable agents; and (3) the Introspector, which refines the agent’s temporal strategies via semantic gradient descent after executing each time-step action. Our main contributions are summarized as follows:

- **Insightfully.** To the best of our knowledge, this is the first LLM-based MAS to tackle partial observability by explicitly decomposing reasoning into spatial and temporal dimensions. We couple semantic reasoning with mean-field statistical features via neighborhood negotiation, enabling robust long-horizon coordination.
- **Technically.** We develop MACRO-LLM, a synergistic architecture comprising three modules: a CoProposer for future unobservability, a Negotiator for spatial partial observability, and an Introspector for historical partial observability. Together, they facilitate the continuous refinement of spatiotemporal strategies through localized interactions.
- **Experimentally.** We conduct comprehensive experiments on the Cooperative Adaptive Cruise Control (CACC) and Pandemic

Control (PC) tasks, comparing against MARL and LLM-based baselines. Empirical results demonstrate that MACRO-LLM significantly outperforms existing methods, exhibiting superior coordination efficiency, scalability, and robustness against environmental dynamics.

2 Related Works

LLM-based Multi-Agent Systems. Existing LLM-based MAS have evolved from general collaboration frameworks (Li et al., 2023a; Wu et al., 2023) to structured systems with persistent memory and reasoning capabilities (Hong et al., 2023; Wang et al., 2023). To address spatial partial observability, recent works adopt either *hierarchical aggregation*, which centralizes information flow (Yu et al., 2024; Estornell et al., 2025), or *belief-based inference*, which deduces hidden states via reasoning chains (Li et al., 2023b; Davidson et al., 2024). However, these approaches often rely on ideal communication bandwidth or static topologies, failing to account for the dynamic coupling of spatial dispersion and temporal uncertainty. MACRO-LLM fills this gap by enabling decentralized spatiotemporal reasoning without reliance on central nodes or global views.

Multi-Agent Reinforcement Learning. Traditional approaches address partial observability via the Dec-POMDP framework (Oliehoek et al., 2016; Koops et al., 2024), often utilizing Centralized Training with Decentralized Execution (CTDE) (Kia et al., 2024; Bernstein et al., 2005) or Mean-Field approximations (Yang et al., 2018; Ganapathi Subramanian et al., 2020) to enhance scalability. While algorithms like MAPPO (Schulman et al., 2017), DMPO (Ma et al., 2024), and communication-aware methods like IC3Net (Singh et al., 2018) improve stability, they remain computationally intensive and environment-specific. They require costly retraining when transferring to new scenarios due to poor generalization (Huh and Mopathra, 2023; Oroojlooy and Hajinezhad, 2023). In contrast, our framework leverages LLMs to achieve zero-shot generalization without parameter updates. Due to space constraints, we provide an extended review in Appendix A.

3 MACRO-LLM Framework

MACRO-LLM establishes a decentralized negotiation framework for MAS operating under spatiotemporal partial observability. As illustrated in

Fig. 2, the architecture of agent n comprises three synergistic modules: (1) **CoProposer**, for collaborative proposal generation; (2) **Negotiator**, for conflict resolution and spatial strategy updates; and (3) **Introspector**, for temporal strategy refinement via semantic gradient descent.

3.1 System Overview

We model the MAS as a peer-to-peer graph $\mathcal{G} = (\mathcal{V}, \mathcal{E})$, where \mathcal{V} denotes the set of agents and \mathcal{E} represents the communication links. For any agent $n \in \mathcal{V}$, its neighborhood is defined as $\mathcal{N}_n = \{m \in \mathcal{V} | (n, m) \in \mathcal{E}\}$, consisting of all directly communicable neighbors. Reflecting real-world constraints, the system operates without a central coordinator.

The primary goal is to enable decentralized collaboration that maximizes global performance under local constraints. At initialization, each agent n is provided with a system prompt defining the task, action space, state dynamics, and reward criteria.

3.2 CoProposer

The CoProposer module generates high-quality action proposals by integrating long-term objectives with immediate spatial constraints. At time step t , agent n constructs a collaborative proposal P_n^t , comprising actions for itself and its observable neighbors \mathcal{N}_n for subsequent negotiation.

Temporal Strategy Formulation. To align short-term decisions with global objectives despite incomplete information, we introduce a high-level temporal strategy. Agent n derives this strategy based on its current observation o_n^t , action space \mathcal{A}_n , and global objectives \mathcal{J}^{global} . This produces a macroscopic plan $\Pi_{n,t}^{temp} = \text{LLM}(o_n^t, \mathcal{A}_n, \mathcal{J}^{global})$, guiding step-by-step progression toward the goal.

Spatial Strategy Formulation. To incorporate spatial context, agent n infers potential cascading effects originating from unobservable agents. By analyzing its local observation o_n^t and the network topology \mathcal{G} , the agent forecasts multi-agent dynamics to formulate a spatial strategy $\Pi_{n,t}^{spatial} = \text{LLM}(o_n^t, \mathcal{G})$.

Proposal Generation via Rollout-Simulated Verification. Leveraging current spatial and temporal strategies, agent n first generates an initial proposal $P_n^{t,0} = (o_n^t, a_n^{t,0}, \{a_{n \rightarrow m}^{t,0}\})$ by identifying the most advantageous action for itself and inferring cooperative actions for its neighbors \mathcal{N}_n . Due

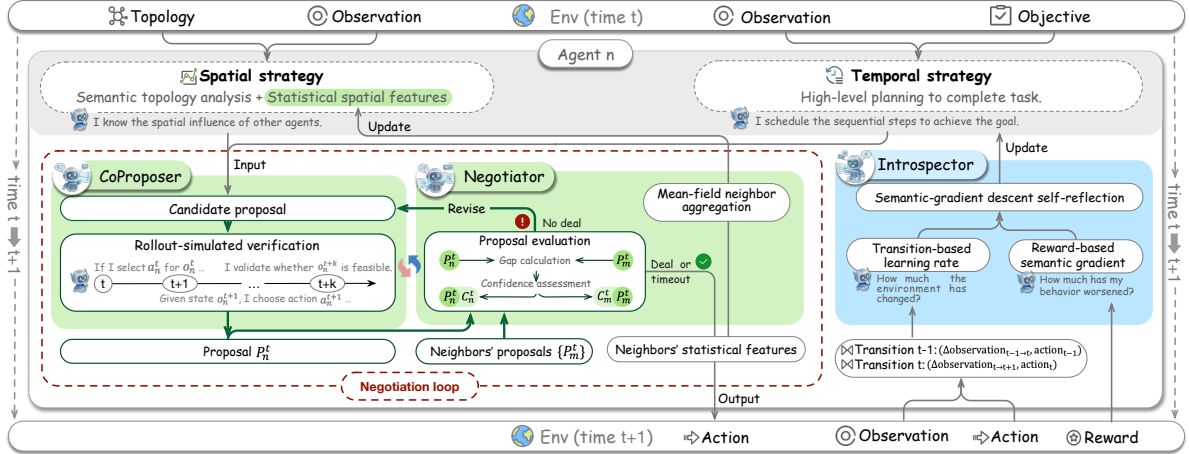


Figure 2: Architecture of MACRO-LLM for agent n . The framework comprises three synergistic modules: (1) the CoProposer generates proposals; (2) the Negotiator handles conflict resolution and spatial strategy updates; and (3) the Introspector performs strategy refinement. The CoProposer and Negotiator form a negotiation loop to process observations at time t and output coordinated actions, leading to the next observation at $t + 1$.

to future uncertainty, this proposal requires validation through rollout-simulated verification. Agent n first predicts its next observation $o_n^{t+1,0}$ and assesses whether this predicted future state constitutes an improvement to evaluate the proposal’s effectiveness. Then, this process iterates between proposal generation and next-observation verification over k time steps, constituting a rollout.

Rollout: *In our framework, a rollout is a multi-step simulation from time t to $t + k$ that projects agent n ’s future states and actions under its current strategy. The sequence of observations, actions, and rewards across these k steps forms a trajectory, denoted as*

$$\tau_n = \left((o_n^t, a_n^t, R_n^t), \dots, (o_n^{t+k}, a_n^{t+k}, R_n^{t+k}) \right). \quad (1)$$

To evaluate a rollout, we employ a progressive constraint relaxation mechanism. For the immediate step (t), the action must strictly satisfy all environmental constraints to ensure safety. For subsequent steps ($t + 1$ to $t + k$), considering increasing uncertainty, criteria are relaxed to minimum viability constraints. This ensures the action a_n^t is safe while conducive to future positive outcomes. The estimated cumulative reward is formulated as:

$$\mathcal{R}(\tau_n) = \sum_{\iota=0}^k \gamma^\iota R_n(o_n^{t+\iota}, a_n^{t+\iota}). \quad (2)$$

To reduce computational complexity over long horizons, reward signal beyond $t + 1$ is simplified to a binary indicator ($r = 1$ if constraints are met, else 0). If a proposal violates constraints during

the rollout, agent n revises its action to generate a new candidate. This cycle repeats until a valid proposal is found or the maximum attempt limit is reached, at which point the candidate with the highest $\mathcal{R}(\tau_n)$ is selected and broadcast to neighbors. This phase ensures each agent’s initial proposal maintains temporal consistency and spatial awareness for effective collaboration. The pseudocode is provided in [Appendix B](#).

3.3 Negotiator

In decentralized environments, agents often generate proposals concurrently. Consequently, an agent must broadcast its own intent while processing incoming proposals from neighbors. This concurrency introduces conflicting actions, necessitating a negotiation mechanism to resolve conflicts and coordinate actions.

Neighborhood State Aggregation via Mean-Field Approximation. To extend agents’ perception beyond observable limits, we complement semantic reasoning with statistical state features. In complex topologies, exchanging raw observations is inefficient due to bandwidth constraints. To address this, we introduce a protocol based on mean-field approximation (Yang et al., 2018) to transmit aggregated statistical features.

The core idea of mean-field theory approximates complex pairwise interactions between an individual and all other agents in the environment can be approximated by the interaction between the individual and an aggregated “mean field” effect (Lasry and Lions, 2007). Accordingly, we represent the

neighborhood influence through weighted statistics. For an agent n , the state s_m^t of a neighbor m is decomposed into a local mean field and a fluctuation term:

$$s_m^t = \mu_n + \delta s_{n \rightarrow m}^t, \quad \mu_n = \frac{\sum_{m \in \mathcal{N}_n} w_{n,m} s_m^t}{\sum_{m \in \mathcal{N}_n} w_{n,m}}, \quad (3)$$

where μ_n represents the weighted mean of the neighborhood's spatial features. The weighted variance is defined as:

$$\sigma_n^2 = \frac{\sum_{m \in \mathcal{N}_n} w_{n,m} (s_m^t - \mu_n)^2}{\sum_{m \in \mathcal{N}_n} w_{n,m}}. \quad (4)$$

Here, weights $w_{n,m} > 0$ are determined by domain-specific relational factors, such as the spatial distance between agents. During negotiation, agents transmit these statistical features instead of raw data to characterize unobservable contexts. Once agent n receives statistical features (μ_m, σ_m^2, W_m) from a neighbor m , it updates the aggregated features incorporating its own state s_n^t (with weight w_n) using the weighted Welford algorithm (Welford, 1962). This enables computationally efficient updates in one operation, the update equation is provided in [Appendix C](#).

Proposal Confidence Assessment. To evaluate proposal reliability, agent n computes the pairwise differences between its own proposal P_n^t and received neighbor proposals $\{P_m^t\}_{m \in \mathcal{N}_n}$. Local consensus is achieved if all differences fall below a predefined threshold ϵ . Note that due to overlapping communication ranges, global consensus is only achieved when all agents in the network have reached local consensus and the negotiation is terminated. If consensus is not met, the agent analyzes the root causes of discrepancies, updates its spatial strategy by incorporating the received mean-field states, and assigns confidence weights to each neighbor's proposal.

Proposal Regeneration. The agent generates a refined proposal by integrating its original proposal with the weighted neighbor proposals, using the assigned confidence weights. This refined proposal then undergoes rollout verification as detailed in [Sec. 3.2](#).

Multi-Round Negotiation. A complete iteration of the CoProposer ([Sec. 3.2](#)) and Negotiator ([Sec. 3.3](#)) constitutes a *negotiation round*. MACRO-LLM typically performs r rounds to exchange statistical features and proposals. Upon completion,

agent n synthesizes the proposal evolution to make a final confidence-weighted decision.

3.4 Introspector

Due to spatiotemporal partial observability, an agent's state inference is often compromised by dynamic environmental shifts and the unpredictable behaviors of others. Consequently, if an agent observes a reward decline between time steps, it initiates a *self-reflection mechanism* to analyze whether substantial environmental changes have occurred. We model this process as a *Semantic Gradient Descent*, utilizing the reward gap as a signal to update spatiotemporal strategies.

Observation-Consistency-based Adaptive Learning Rate.

We first quantify the magnitude of environmental shifts to determine the "step size" for strategy updates. Let o_n^t denote the vectorized observation of agent n at time t . We construct a transition vector Γ_n^t by concatenating the observation difference and the action vector, defined as $\Gamma_n^t = (\Delta o_n^t, a_n^t)$, where $\Delta o_n^t = o_n^{t+1} - o_n^t$.

To evaluate scene consistency, we compute the cosine similarity between two consecutive transitions, Γ_n^{t-1} and Γ_n^t . The *reflection learning rate* (lr) is derived from scene discontinuity:

$$lr = 1 - \frac{\Gamma_n^{t-1} \cdot \Gamma_n^t}{\|\Gamma_n^{t-1}\| \cdot \|\Gamma_n^t\|}. \quad (5)$$

Here, $lr \in [0, 2]$ is a scalar inversely proportional to transition similarity. A higher lr indicates a drastic environmental shifts, requiring aggressive strategy updates, whereas a lower lr implies minor fluctuations, requiring only fine-grained refinements.

Semantic Gradient Computation.

Inspired by textual gradient descent (Yuksekgonul et al., 2025), we formalize the *semantic gradient* as a natural language description of the "direction" for strategic improvement. By analyzing observation logs and negotiation records \mathbf{N} (where \mathbf{N}_t denotes the negotiation history at time t), the agent identifies the root cause of the performance drop. The semantic gradient is generated via: $g_{n,t}^{\text{semantic}} = \text{LLM}(\Gamma_n^{t-1}, \Gamma_n^t, \Delta R_n^t, \Pi_n^{\text{temp}}, \Pi_n^{\text{spatial}}, \mathbf{N}_{t-1}, \mathbf{N}_t)$. Here, $g_{n,t}^{\text{semantic}}$ represents textual rules that explain the causal links between actions, state changes, and negative reward outcomes, effectively pointing out the flaws in the current strategy.

Table 1: Performance comparison on the CACC task across *Catch-up* and *Slow-down* scenarios. Metrics include RMSE and SD for Headway (H) and Velocity (V). **Bold** and underline indicate best and second-best results, respectively.

Scenario 1: Catch-up				
Methods	RMSE-H (↓)	RMSE-V (↓)	SD-H (↓)	SD-V (↓)
ToM-Belief	5.514	4.409	4.002	3.130
ChatEval	5.495	2.113	2.947	1.241
LAMEN	1.891	<u>0.648</u>	3.320	0.601
DPPO	<u>1.603</u>	0.978	<u>0.994</u>	<u>0.474</u>
DMPO	4.765	0.534	3.025	1.349
IC3Net	8.687	4.205	7.232	3.399
MACRO-LLM	1.212	0.897	0.455	0.283
Scenario 2: Slow-down				
Methods	RMSE-H (↓)	RMSE-V (↓)	SD-H (↓)	SD-V (↓)
ToM-Belief	0.641	4.681	<u>0.225</u>	<u>0.480</u>
ChatEval	3.062	5.708	0.778	1.016
LAMEN	<u>0.923</u>	3.385	0.635	0.750
DPPO	1.720	<u>3.121</u>	1.410	1.176
DMPO	2.226	3.059	1.742	1.189
IC3Net	7.877	4.678	5.207	2.319
MACRO-LLM	0.561	3.325	0.209	0.345

Strategy Update. Finally, we update the temporal strategy using the computed gradient and learning rate. The update rule is conceptually formulated as:

$$\Pi_{n,t+1}^{\text{temp}} \leftarrow \Pi_{n,t}^{\text{temp}} - lr \cdot g_{n,t}^{\text{semantic}}. \quad (6)$$

Equation (6) represents a prompt-based operation where the scalar lr modulates the instruction intensity: a high lr prompts the LLM to "discard and rewrite" the strategy based on $g_{n,t}^{\text{semantic}}$, while a low lr implies a "fine-grained refinement" of the existing $\Pi_{n,t}^{\text{temp}}$. This process completes the semantic learning loop, enabling MACRO-LLM to adapt to dynamic environments by emulating stochastic gradient descent within the semantic strategy space.

4 Experiments

We evaluate MACRO-LLM on two distinct interactive tasks requiring complex multi-turn coordination under partial observability: Cooperative Adaptive Cruise Control (CACC) (Chu et al., 2020) and Pandemic Control (PC) (Kompella* et al., 2020).

4.1 Experimental Settings

Implementation Details. We implement the MACRO-LLM framework using GPT-4o (gpt-4o-2024-08-06) via the OpenAI API with the openai Python library (version 1.75.0). To ensure focused reasoning and reproducibility, we set the sampling temperature to 0.3 and top-p to 1.0. All simulation

environments and local baselines (e.g., MARL algorithms) were executed on a server equipped with 4 NVIDIA GeForce RTX 3090 GPUs. Detailed prompt templates are provided in [Appendix J](#).

Task Configurations. We evaluate MACRO-LLM across two diverse domains requiring complex coordination. (1) *CACC*: A continuous vehicle platooning task where a fleet of agents (default $N = 8$) must maintain safety and efficiency during dynamic "Catch-up" and "Slow-down" scenarios under partial observability. (2) *Pandemic Control (PC)*: A strategic planning task where agents (buildings) regulate mobility to mitigate virus spread across three urban topologies (Helsinki, Hong Kong, and New York). These tasks evaluate the framework's capability in both fine-grained control and long-horizon strategic planning. Refer to [Appendix D](#) for detailed simulator configurations and city topologies.

Baselines. We benchmark MACRO-LLM against representative methods from two paradigms: (1) *LLM-based MAS baselines*: We select representative frameworks including ToM-Belief (Li et al., 2023b), ChatEval (Chan et al., 2023), and LAMEN (Davidson et al., 2024); and (2) *MARL baselines*: We select representative MARL algorithms including DPPO, DMPO (Ma et al., 2024), and IC3Net (Singh et al., 2018). Details on baseline implementations, prompt adaptations, and fair comparison settings are provided in [Appendix E](#).

Evaluation Metrics. For the CACC task, we evaluate platoon stability via the Root Mean Square Error (RMSE) and Standard Deviation (SD) of both velocity and headway distance (denoted as RMSE-V/H and SD-V/H). For the PC task, we assess containment efficacy through Normalized Infection (I_n), Peak Infection (PI_n), Normalized Death (D_n) and total Pandemic Duration (PD). Metric definitions are detailed in [Appendix F](#).

4.2 Performance of CACC Tasks

Based on the experimental results presented in Table 1, MACRO-LLM demonstrates superior coordination capabilities, particularly in enhancing platoon stability and consistency compared to both MARL-based and LLM-based baselines. (1) In the **Catch-up** scenario, MACRO-LLM reduces the SD-H by 86.3% compared to LAMEN and 54.2% compared to DPPO. Furthermore, it significantly improves tracking precision, reducing RMSE-H

Table 2: Performance comparison on the PC task across Helsinki, Hong Kong, and New York topologies. Metrics include Normalized Infection (I_n), Peak Infection (PI_n), Normalized Dead (D_n), and Pandemic Duration (PD). **Bold** and underline indicate best and second-best results, respectively.

Methods	Helsinki				Hong Kong				New York			
	$I_n (\downarrow)$	$PI_n (\downarrow)$	$D_n (\downarrow)$	PD (\downarrow)	$I_n (\downarrow)$	$PI_n (\downarrow)$	$D_n (\downarrow)$	PD (\downarrow)	$I_n (\downarrow)$	$PI_n (\downarrow)$	$D_n (\downarrow)$	PD (\downarrow)
DPPO	0.426	0.110	0.007	62	0.370	0.083	0.004	83	0.923	0.363	0.009	95
DMPO	0.010	0.008	<u>0.001</u>	<u>13</u>	0.271	0.057	0.003	59	0.332	0.109	0.002	53
IC3Net	0.651	0.186	0.009	69	0.259	0.067	0.003	52	0.789	0.284	0.007	93
ToM-Belief	0.184	0.042	0.002	92	0.239	0.028	0.003	120	0.130	0.023	0.001	60
ChatEval	0.010	0.008	0.000	42	0.009	0.003	<u>0.001</u>	24	0.290	0.043	0.002	83
LAMEN	0.010	0.008	0.002	17	0.012	<u>0.005</u>	0.000	<u>23</u>	0.164	0.025	0.002	<u>52</u>
MACRO-LLM	0.010	0.008	0.000	9	0.006	<u>0.005</u>	0.000	22	0.005	0.003	0.000	33

Table 3: Generalizability analysis of MACRO-LLM across different LLM backbones. S1/S2: CACC Catch-up/Slow-down scenarios. C1-C3: PC topologies for Helsinki, Hong Kong, and New York.

Tasks	Base Models	Metrics (\downarrow)			
		RMSE-H	RMSE-V	SD-H	SD-V
CACC	S1	DeepSeek-V3.1	1.528	0.553	0.611
		Qwen3-flash	3.521	1.910	2.935
		GPT-4o-mini	2.906	1.667	1.858
		GPT-4o	1.212	0.897	0.455
	S2	DeepSeek-V3.1	0.649	3.388	0.274
		Qwen3-flash	3.871	3.678	2.946
		GPT-4o-mini	2.352	3.999	1.598
		GPT-4o	0.561	3.325	0.209
Tasks	Base Models	I_n	PI_n	D_n	PD
PC	C1	DeepSeek-V3.1	0.098	0.038	0.002
		Qwen3-flash	0.010	0.008	0.002
		GPT-4o-mini	0.010	0.010	0.000
		GPT-4o	0.010	0.008	0.000
	C2	DeepSeek-V3.1	0.008	0.005	0.001
		Qwen3-flash	0.008	0.006	0.001
		GPT-4o-mini	0.006	0.004	0.000
		GPT-4o	0.006	0.005	0.001
	C3	DeepSeek-V3.1	0.003	0.003	0.000
		Qwen3-flash	0.003	0.003	0.000
		GPT-4o-mini	0.003	0.003	0.000
		GPT-4o	0.005	0.003	0.000

by 24.4% relative to DPPO. This indicates that the negotiation mechanism of MACRO-LLM effectively mitigates the oscillations observed in baselines, resulting in smoother and safer acceleration phases. (2) In the **Slow-down** scenario, the results highlight a strategic trade-off where MACRO-LLM prioritizes headway maintenance for safety over aggressive velocity matching. While maintaining competitive velocity errors, our framework substantially outperforms baselines in maintaining safe distances. MACRO-LLM improves SD-V by 28.1% over the ToM-Belief. These results collectively validate that MACRO-LLM ensures robust

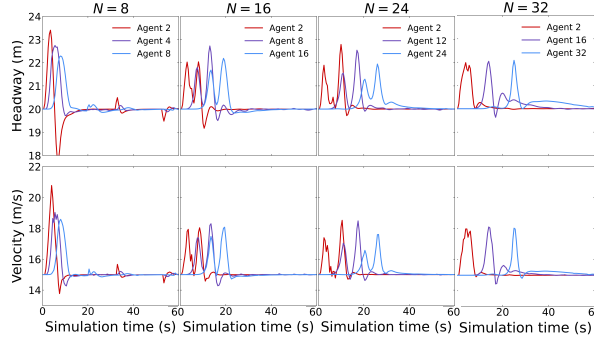


Figure 3: Scalability analysis of MACRO-LLM on the CACC task for number of agents $N \in \{8, 16, 24, 32\}$.

performance.

4.3 Performance on PC Tasks.

Table 2 presents the comparative results across three distinct city topologies: **Helsinki**, **Hong Kong**, and **New York**. MACRO-LLM consistently demonstrates superior containment efficacy, achieving the lowest normalized infection rates (I_n) and peak infections (PI_n) while significantly shortening the pandemic duration (PD) across all settings. Specifically, in the most complex **New York** scenario, MACRO-LLM significantly outperforms DPPO, reducing cumulative infections by over 99.2% and shortening the pandemic duration by nearly 3 times compared to DPPO. This indicates that our framework effectively balances peak suppression with rapid containment across varying population scales. Notably, while baselines often struggle with the trade-off between strict containment and duration, MACRO-LLM optimizes both simultaneously. For instance, in Hong Kong, while LAMEN achieves low infection rates, MACRO-LLM further reduces the pandemic duration, demonstrating more efficient long-term planning. This robust performance highlights the

critical role of the Negotiator and Introspector modules in handling complex, large-scale coordination.

4.4 Analysis of Model Generalizability

We investigate the robustness of MACRO-LLM by instantiating it with diverse LLM backbones, including GPT-4o-mini, Qwen3-flash (Bai et al., 2023), GPT-4o, and DeepSeek-V3.1 (Liu et al., 2024). The results are shown in Table 3. For the precision-critical CACC task, fine-grained spatial control is heavily influenced by the reasoning capability of the base model. Powerful models like GPT-4o and DeepSeek-V3.1 significantly reduce RMSE-H by over 47.4% in the Catch-up scenario (S1) compared to GPT-4o-mini. Conversely, in the PC task, Qwen3-flash achieves containment efficacy comparable to GPT-4o. This demonstrates that MACRO-LLM effectively compensates for the limitations of smaller models in strategic planning tasks, demonstrating the framework’s robustness and feasibility across various computational budgets.

4.5 Analysis of Scalability

To investigate the scalability of MACRO-LLM, we extended the CACC Catch-up scenario to varying fleet sizes of $N \in \{8, 16, 24, 32\}$, analyzing the headway and velocity trajectories of representative agents located at the front, middle, and rear of the platoon. As illustrated in Figure 3, MACRO-LLM maintains consistent robustness to increasing fleet sizes, even as the network quadruples to $N = 32$. While the propagation delay naturally increases with platoon size, the oscillation amplitudes remain bounded and effectively damped over time. All agents, regardless of their position, converge to the target equilibrium within 40s. By compressing the dense interactions of a large-scale network into aggregated statistical features, each agent only needs to process a fixed-size local context and a virtual mean-field node, thereby mitigating communication overhead and contextual overload. The results demonstrate that MACRO-LLM effectively balances local precision with global coherence, ensuring scalability for large-scale deployment. More analysis about scalability and cost (including communication and computation cost) are provided in Appendix G.

4.6 Ablation Study

We validate the contribution of each module in Figs. 4 and 5. As shown in Fig. 4, removing

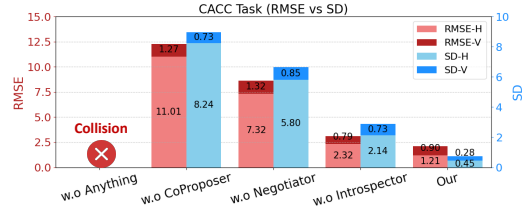


Figure 4: Ablation of MACRO-LLM—impact of each module on CACC performance.

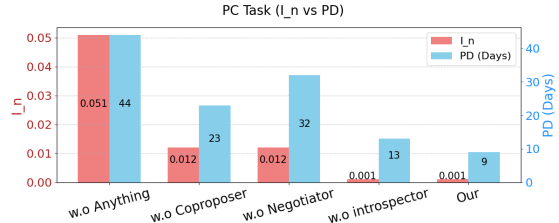


Figure 5: Ablation of MACRO-LLM—impact of each module on PC performance

the CoProposer leads to immediate coordination failure, resulting in collisions in CACC. Ablating the Negotiator causes stability metrics to degrade drastically, demonstrating that unstructured communication fails to resolve conflicting intentions. Furthermore, without the Introspector, agents struggle to suppress oscillations over time due to the lack of self-reflection. In the PC task (Fig. 5), this manifests as longer PD and higher I_n . Comprehensive quantitative analyses are provided in Appendix H.

5 Conclusion

In this work, we present MACRO-LLM, a novel framework enabling agents to reason and coordinate through localized negotiations under spatiotemporal partial observability. We explicitly decompose the coordination challenge along spatial and temporal dimensions, addressing them through three interconnected modules: (1) a CoProposer to generate collaborative actions and mitigate future uncertainty via predictive rollouts; (2) a Negotiator that resolves spatial conflicts using mean-field statistical estimations; and (3) an Introspector that facilitates strategic refinement via semantic gradient descent. Extensive experiments on CACC and PC tasks demonstrate MACRO-LLM’s capability to align local actions with long-term global objectives, achieving superior collaborative efficiency compared to representative baselines. Ultimately, our work highlights the critical role of explicitly modeling spatiotemporal dynamics in scaling LLM-based multi-agent systems.

Limitations

While MACRO-LLM demonstrates robust coordination capabilities, we acknowledge two primary limitations. First, the iterative negotiation mechanism introduces computational overhead and latency, necessitating a trade-off between reasoning depth and inference speed for time-sensitive applications. The theoretical communication and computation cost analyses are provided in **Appendix G**. Second, relying on foundation model APIs requires additional context injection for domain adaptation, which increases token consumption and inference costs. Future work will explore lightweight fine-tuning or Retrieval-Augmented Generation (RAG) to internalize domain knowledge, thereby enhancing execution efficiency and reducing context dependency.

References

Emile Anand, Ishani Karmarkar, and Guannan Qu. 2024. Mean-field sampling for cooperative multi-agent reinforcement learning. *CoRR*.

Jinze Bai, Shuai Bai, Yunfei Chu, Zeyu Cui, Kai Dang, Xiaodong Deng, Yang Fan, Wenbin Ge, Yu Han, Fei Huang, and 1 others. 2023. Qwen technical report. *arXiv preprint arXiv:2309.16609*.

Daniel S Bernstein, Eric A Hansen, and Shlomo Zilberman. 2005. Bounded policy iteration for decentralized pomdps. In *Proceedings of the nineteenth international joint conference on artificial intelligence (IJCAI)*, pages 52–57.

Maciej Besta, Nils Blach, Ales Kubicek, Robert Gerstenberger, Michal Podstawski, Lukas Gianinazzi, Joanna Gajda, Tomasz Lehmann, Hubert Niewiadomski, Piotr Nyczek, and 1 others. 2024. Graph of thoughts: Solving elaborate problems with large language models. In *Proceedings of the AAAI conference on artificial intelligence*, volume 38, pages 17682–17690.

Chi-Min Chan, Weize Chen, Yusheng Su, Jianxuan Yu, Wei Xue, Shanghang Zhang, Jie Fu, and Zhiyuan Liu. 2023. Chateval: Towards better llm-based evaluators through multi-agent debate. *International Conference on Learning Representations*.

Tony F Chan, Gene H Golub, and Randall J LeVeque. 1983. Algorithms for computing the sample variance: Analysis and recommendations. *The American Statistician*, 37(3):242–247.

Handi Chen, Weipeng Deng, Shuo Yang, Jinfeng Xu, Zhihan Jiang, Edith C. H. Ngai, Jiangchuan Liu, and Xue Liu. 2025. Toward edge general intelligence via large language models: Opportunities and challenges. *IEEE Network*, 39(5):263–271.

Tianshu Chu, Sandeep Chinchali, and Sachin Katti. 2020. Multi-agent reinforcement learning for networked system control. *International Conference on Learning Representations*.

Hao Cui, Zahra Shamsi, Gowoon Cheon, Xuejian Ma, Shutong Li, Maria Tikhanovskaya, Peter Christian Norgaard, Nayantara Mudur, Martyna Beata Plomecka, Paul Raccuglia, Yasaman Bahri, Victor V. Albert, Pranesh Srinivasan, Haining Pan, Philippe Faist, Brian A Rohr, Michael J. Statt, Dan Morris, Drew Purves, and 11 others. 2025. CURIE: Evaluating LLMs on multitask scientific long-context understanding and reasoning. In *The Thirteenth International Conference on Learning Representations*.

Tim R Davidson, Veniamin Veselovsky, Martin Jofoski, Maxime Peyrard, Antoine Bosselut, Michal Kosinski, and Robert West. 2024. Evaluating language model agency through negotiations. *International Conference on Learning Representations*.

Charles Desjardins and Brahim Chaib-draa. 2011. Cooperative adaptive cruise control: A reinforcement learning approach. *IEEE Transactions on Intelligent Transportation Systems*, 12(4):1248–1260.

Andrew Estornell, Jean-Francois Ton, Muhammad Faaiz Taufiq, and Hang Li. 2025. How to train a leader: Hierarchical reasoning in multi-agent llms. *arXiv preprint arXiv:2507.08960*.

Sriram Ganapathi Subramanian, Pascal Poupart, Matthew E Taylor, and Nidhi Hegde. 2020. Multi type mean field reinforcement learning. In *Proceedings of the 19th International Conference on Autonomous Agents and MultiAgent Systems*, pages 411–419.

Haotian Gu, Xin Guo, Xiaoli Wei, and Renyuan Xu. 2025. Mean-field multiagent reinforcement learning: A decentralized network approach. *Mathematics of Operations Research*, 50(1):506–536.

Sirui Hong, Mingchen Zhuge, Jonathan Chen, Xiawu Zheng, Yuheng Cheng, Jinlin Wang, Ceyao Zhang, Zili Wang, Steven Ka Shing Yau, Zijuan Lin, and 1 others. 2023. Metagpt: Meta programming for a multi-agent collaborative framework. In *The Twelfth International Conference on Learning Representations*.

Zhipeng Hou, Junyi Tang, and Yipeng Wang. 2025. Halo: Hierarchical autonomous logic-oriented orchestration for multi-agent llm systems. *arXiv preprint arXiv:2505.13516*.

Xu Huang, Weiwen Liu, Xiaolong Chen, Xingmei Wang, Hao Wang, Defu Lian, Yasheng Wang, Ruiming Tang, and Enhong Chen. 2024. Understanding the planning of llm agents: A survey. *arXiv preprint arXiv:2402.02716*.

Dom Huh and Prasant Mohapatra. 2023. Multi-agent reinforcement learning: A comprehensive survey. *arXiv preprint arXiv:2312.10256*.

Justin Khasentino, Anastasiya Belyaeva, Xin Liu, Zhun Yang, Nicholas A Furlotte, Chace Lee, Erik Schenck, Yojan Patel, Jian Cui, Logan Douglas Schneider, and 1 others. 2025. A personal health large language model for sleep and fitness coaching. *Nature Medicine*, pages 1–10.

Maryam Kia, Jordan Cramer, and Artur Luczak. 2024. Memory augmented multi-agent reinforcement learning for cooperative environment. In *International Conference on Artificial Intelligence and Soft Computing*, pages 92–103. Springer.

Varun Kompella*, Roberto Capobianco*, Stacy Jong, Jonathan Browne, Spencer Fox, Lauren Meyers, Peter Wurman, and Peter Stone. 2020. Reinforcement learning for optimization of covid-19 mitigation policies. *Preprint*, arXiv:2010.10560.

Wietze Koops, Sebastian Junges, and Nils Jansen. 2024. Approximate dec-pomdp solving using multi-agent a. In *Proceedings of the Thirty-Third International Joint Conference on Artificial Intelligence*, pages 6743–6751.

Jean-Michel Lasry and Pierre-Louis Lions. 2007. Mean field games. *Japanese journal of mathematics*, 2(1):229–260.

Chenfei Li, Yujia Liang, Zihan Song, and 1 others. 2023a. Camel: Communicative agents for “mind” exploration of large language model society. *arXiv preprint arXiv:2303.17760*.

Huao Li, Yu Quan Chong, Simon Stepputtis, Joseph Campbell, Dana Hughes, Michael Lewis, and Kaitia Sycara. 2023b. Theory of mind for multi-agent collaboration via large language models. *Empirical Methods in Natural Language Processing*.

Aixin Liu, Bei Feng, Bing Xue, Bingxuan Wang, Bochao Wu, Chengda Lu, Chenggang Zhao, Chengqi Deng, Chenyu Zhang, Chong Ruan, and 1 others. 2024. Deepseek-v3 technical report. *arXiv preprint arXiv:2412.19437*.

Chengdong Ma, Aming Li, Yali Du, Hao Dong, and Yaodong Yang. 2024. Efficient and scalable reinforcement learning for large-scale network control. *Nature Machine Intelligence*, 6(9):1006–1020.

Aman Madaan, Niket Tandon, Prakhar Gupta, Skyler Hallinan, Luyu Gao, Sarah Wiegreffe, Uri Alon, Nouha Dziri, Shrimai Prabhumoye, Yiming Yang, and 1 others. 2023. Self-refine: Iterative refinement with self-feedback. *Advances in Neural Information Processing Systems*, 36:46534–46594.

Frans A Oliehoek, Christopher Amato, and 1 others. 2016. *A concise introduction to decentralized POMDPs*, volume 1. Springer.

Afshin Oroojlooy and Davood Hajinezhad. 2023. A review of cooperative multi-agent deep reinforcement learning. *Applied Intelligence*, 53(11):13677–13722.

Joon Sung Park, Joseph O’Brien, Carrie Jun Cai, Meredith Ringel Morris, Percy Liang, and Michael S. Bernstein. 2023. Generative agents: Interactive simulacra of human behavior. In *Proceedings of the 36th Annual ACM Symposium on User Interface Software and Technology*, UIST ’23, New York, NY, USA. Association for Computing Machinery.

John Schulman, Filip Wolski, Prafulla Dhariwal, Alec Radford, and Oleg Klimov. 2017. Proximal policy optimization algorithms. *arXiv preprint arXiv:1707.06347*.

Yao Shi, Rongkeng Liang, and Yong Xu. 2025. Educationq: Evaluating llms’ teaching capabilities through multi-agent dialogue framework. *Association for Computational Linguistics*.

Amanpreet Singh, Tushar Jain, and Sainbayar Sukhbaatar. 2018. Learning when to communicate at scale in multiagent cooperative and competitive tasks. *International Conference on Learning Representations*.

Bart Van Arem, Cornelie JG Van Driel, and Ruben Visser. 2006. The impact of cooperative adaptive cruise control on traffic-flow characteristics. *IEEE Transactions on intelligent transportation systems*, 7(4):429–436.

Guanzhi Wang, Qian Lin, Zuoqi Chen, and 1 others. 2023. Voyager: An open-ended embodied agent with large language models. *arXiv preprint arXiv:2305.16291*.

Xiaoqiang Wang, Liangjun Ke, Gewei Zhang, and Dapeng Zhu. 2022a. Attention based large scale multi-agent reinforcement learning. In *2022 5th International Conference on Artificial Intelligence and Big Data (ICAIBD)*, pages 112–117. IEEE.

Xuezhi Wang, Jason Wei, Dale Schuurmans, Quoc Le, Ed Chi, Sharan Narang, Aakanksa Chowdhery, and Denny Zhou. 2022b. Self-consistency improves chain of thought reasoning in language models. *arXiv preprint arXiv:2203.11171*.

Zhenhailong Wang, Shaoguang Mao, Wenshan Wu, Tao Ge, Furu Wei, and Heng Ji. 2024. Unleashing the emergent cognitive synergy in large language models: A task-solving agent through multi-persona self-collaboration. In *Proceedings of the 2024 Conference of the North American Chapter of the Association for Computational Linguistics: Human Language Technologies (Volume 1: Long Papers)*, pages 257–279, Mexico City, Mexico. Association for Computational Linguistics.

Zixiang Wang, Yinghao Zhu, Huiya Zhao, Xiaochen Zheng, Dehao Sui, Tianlong Wang, Wen Tang, Yasha Wang, Ewen Harrison, Chengwei Pan, Junyi Gao, and Liantao Ma. 2025. Colacare: Enhancing electronic health record modeling through large language model-driven multi-agent collaboration. In *Proceedings of the ACM on Web Conference 2025*, WWW ’25, page 2250–2261, New York, NY, USA. Association for Computing Machinery.

Jason Wei, Xuezhi Wang, Dale Schuurmans, Maarten Bosma, Fei Xia, Ed Chi, Quoc V Le, Denny Zhou, and 1 others. 2022. Chain-of-thought prompting elicits reasoning in large language models. *Advances in neural information processing systems*, 35:24824–24837.

Barry Payne Welford. 1962. Note on a method for calculating corrected sums of squares and products. *Technometrics*, 4(3):419–420.

Tianyu Wu, Zhuosheng Wang, and 1 others. 2023. Autogen: Enabling next-gen llm applications via multi-agent conversation frameworks. *International Conference on Learning Representations*.

Yaodong Yang, Rui Luo, Minne Li, Ming Zhou, Weinan Zhang, and Jun Wang. 2018. Mean field multi-agent reinforcement learning. In *International conference on machine learning*, pages 5571–5580. PMLR.

Andrew Chi-Chih Yao. 1979. Some complexity questions related to distributive computing (preliminary report). In *Proceedings of the eleventh annual ACM symposium on Theory of computing*, pages 209–213.

Shunyu Yao, Jeffrey Zhao, Dian Yu, Nan Du, Izhak Shafran, Karthik Narasimhan, and Yuan Cao. 2023. React: Synergizing reasoning and acting in language models. In *International Conference on Learning Representations (ICLR)*.

Yangyang Yu, Zhiyuan Yao, Haohang Li, Zhiyang Deng, Yuechen Jiang, Yupeng Cao, Zhi Chen, Jordan Su-chow, Zhenyu Cui, Rong Liu, and 1 others. 2024. Fincon: A synthesized llm multi-agent system with conceptual verbal reinforcement for enhanced financial decision making. *Advances in Neural Information Processing Systems*, 37:137010–137045.

Mert Yuksekgonul, Federico Bianchi, Joseph Boen, and 1 others. 2025. Optimizing generative ai by backpropagating language model feedback. *Nature*, 639:609–616.

Hongxin Zhang, Weihua Du, Jiaming Shan, Qinhong Zhou, Yilun Du, Joshua B. Tenenbaum, Tianmin Shu, and Chuang Gan. 2024. Building cooperative embodied agents modularly with large language models.

Running Zhao, Zhihan Jiang, Xinchen Zhang, Chirui Chang, Handi Chen, Weipeng Deng, Luyao Jin, Xiaojuan Qi, Xun Qian, and Edith C.H. Ngai. 2025. Noteit: A system converting instructional videos to interactable notes through multimodal video understanding. In *Proceedings of the 38th Annual ACM Symposium on User Interface Software and Technology, UIST ’25*, New York, NY, USA. Association for Computing Machinery.

Wanjun Zhong, Lianghong Guo, Qiqi Gao, He Ye, and Yanlin Wang. 2024. Memorybank: Enhancing large language models with long-term memory. In *Proceedings of the AAAI Conference on Artificial Intelligence*, volume 38, pages 19724–19731.

Xinyu Zhu, Junjie Wang, Lin Zhang, Yuxiang Zhang, Yongfeng Huang, Ruyi Gan, Jiaxing Zhang, and Yujiu Yang. 2023. Solving math word problems via cooperative reasoning induced language models. In *Proceedings of the 61st Annual Meeting of the Association for Computational Linguistics*, pages 4471–4485, Toronto, Canada. Association for Computational Linguistics.

Henry Peng Zou, Wei-Chieh Huang, Yaozu Wu, Yankai Chen, Chunyu Miao, Hoang Nguyen, Yue Zhou, Weizhi Zhang, Liancheng Fang, Langzhou He, and 1 others. 2025. Llm-based human-agent collaboration and interaction systems: A survey. *arXiv preprint arXiv:2505.00753*.

A Extended Related Works

Due to space constraints, we provide a comprehensive review of the literature in this appendix.

Agent Planning with LLMs. There has been a recent surge in research on the reasoning, planning, and decision-making capabilities of LLMs to construct agents across diverse domains (Huang et al., 2024). Early works, such as Chain-of-Thought (CoT) (Wei et al., 2022) and ReAct (Yao et al., 2023), enhance reasoning by decomposing complex tasks into subtasks. Another common approach involves generating a broader set of candidate plans through multiple reasoning steps to widen the exploration of possible solutions such as Self-Consistency (Wang et al., 2022b) and Graph-of-Thought (Besta et al., 2024). To further strengthen reasoning, Self-Refine (Madaan et al., 2023) applies self-reflection module, prompting agents to critique failures and iteratively update strategies. To enhance reasoning with historical knowledge, MemoryBank (Zhong et al., 2024) leverages memory-augmented planning to retrieve relevant knowledge and past experiences for guiding decision-making. These diverse methods can be integrated into one agent pipeline to collectively enhance overall capacity. Nevertheless, integrating multiple sophisticated components often incurs high computational costs and can be constrained by context length limitations, potentially undermining coherence in long-horizon tasks.

Extended Related Work on LLM-based Multi-Agent Systems. The emergence of Large Language Models (LLMs) has revolutionized multi-agent collaboration. Early frameworks such as CAMEL (Li et al., 2023a) and AutoGen (Wu et al., 2023) demonstrated the potential of communicative agents to solve open-ended tasks through dynamic role-playing. Subsequent systems introduced structured enhancements to improve stability and capability. For instance, MetaGPT (Hong et al., 2023) incorporates Standardized Operating Procedures (SOPs) to streamline workflows, while Voyager (Wang et al., 2023) utilizes an iterative curriculum with persistent code libraries for embodied control. Despite their success in observable environments (e.g., software engineering, Minecraft), these frameworks typically operate under the assumption of global observability or unrestricted communication, rendering them less effective in spatially distributed, bandwidth-constrained real-

world scenarios. Recent research targeting the information imbalance caused by spatial constraints generally falls into two categories:

(1) Hierarchical aggregation: Works such as FinCon (Yu et al., 2024), MLPO (Estornell et al., 2025), and HALO (Hou et al., 2025) employ hierarchical architectures. These systems designate specific agents (e.g., central hubs) to aggregate incomplete information, constructing a pseudo-global view to compensate for limited local perception. However, this centralization introduces critical bottlenecks: it relies heavily on central nodes and often incurs prohibitive communication overheads as the network scales. (2) Individual reasoning enhancement: A complementary line of research focuses on enhancing individual reasoning capabilities. Theory-of-Mind (ToM) approaches (Li et al., 2023b) enable agents to infer the beliefs and intents of others, while frameworks like LAMEN (Davidson et al., 2024) utilize structured reasoning chains to predict hidden states. While effective for small-scale interactions, these methods often struggle with the *spatiotemporal uncertainty* inherent in complex topologies, where agents must simultaneously reason about spatial neighbors and future dynamics under strict latency constraints.

In contrast, MACRO-LLM proposes a fully decentralized negotiation mechanism that leverages mean-field statistics and semantic strategies, effectively balancing local perception with global coordination goals.

Extended Related Work on MARL To tackle spatial partial observability, the Decentralized Partially Observable Markov Decision Process (Dec-POMDP) serves as the foundational modeling framework (Oliehoek et al., 2016). Under this model, agents must act based on local histories rather than global states. To mitigate the non-stationarity inherent in decentralized learning, the Centralized Training with Decentralized Execution (CTDE) paradigm has become standard. Recent works have further incorporated memory augmentation mechanisms (Kia et al., 2024) and theoretical guarantees (Bernstein et al., 2005) to approximate global state value functions. However, these methods typically require fitting a value function to a specific state space, limiting their transferability.

Scalability remains a critical bottleneck in MARL. Mean-field MARL offers a promising direction by approximating agent-to-agent interactions via the average effect of the neighborhood

(Yang et al., 2018). Subsequent studies have extended this to accommodate agent heterogeneity (Ganapathi Subramanian et al., 2020; Gu et al., 2025) and robustness (Wang et al., 2022a; Anand et al., 2024). Similarly, MACRO-LLM adopts the mean-field principle in its *Negotiator* module to compress spatial information. However, unlike MARL which learns a mean-field policy through extensive episodes, our approach computes mean-field statistical features explicitly as prompts for the LLM, enabling inference-time reasoning without gradient updates.

To improve sample efficiency, advanced policy optimization methods such as Multi-Agent PPO (MAPPO) (Schulman et al., 2017) and Model-based Decentralized Policy Optimization (DMPO) (Ma et al., 2024) have been developed. Furthermore, adaptive communication protocols like IC3Net (Singh et al., 2018) introduce gating mechanisms to decide when to communicate. **Limitations:** Despite these advances, the fundamental reliance on trial-and-error interaction makes MARL computationally intensive (see Fig. 7). As noted by (Huh and Mohapatra, 2023) and (Oroojlooy and Hajinezhad, 2023), MARL policies often struggle to generalize to unseen topologies or agent numbers, necessitating the retraining costs that our LLM-based framework aims to eliminate.

B Detailed Algorithm of Proposal Generation

In this section, we detail the algorithmic procedure for the CoProposer module. The core mechanism, *Proposal Generation via Rollout-Simulated Verification*, is outlined in Algorithm 1.

This process aims to find an action sequence that maximizes cumulative reward while strictly adhering to safety constraints. To ensure computational efficiency, the algorithm employs an *early exit mechanism*: if a generated proposal successfully passes verification over the entire horizon k , it is immediately adopted as the proposal P_n^t , terminating the search loop.

The computational complexity of the CoProposer is dominated by the number of LLM inference calls. Let Att_{\max} be the maximum number of validation attempts and K be the rollout horizon. In the worst-case scenario (where valid proposals are hard to find), the complexity is $\mathcal{O}(Att_{\max} \cdot k)$. To mitigate latency in real-world applications, we set $Att_{\max} = 10$ for all task. The binary simplifi-

cation of rewards beyond $t + 1$ further reduces the overhead of reward calculation.

C Equations for Welford-based State Aggregation

The update rules for the weighted mean and variance are defined as follows:

$$\mu'_n = \mu_m + \frac{w_n}{W_n}(s_n^t - \mu_m), \quad (7)$$

$$\sigma_n^{2'} = \frac{W_m}{W_n}\sigma_m^2 + \frac{w_n}{W_n}(s_n^t - \mu_m)(s_n^t - \mu'_n), \quad (8)$$

where $W_n = W_m + w_n$ represents the updated weight. The aggregated mean μ'_n and variance $\sigma_n^{2'}$ are then abstracted into a textual description of a virtual node within the query prompt, enabling the LLM to analyze trends in the unobserved states. While equations (7) and (8) illustrate the atomic update, in practice, agents apply this iteratively or employ parallel variance merger algorithms (Chan et al., 1983) when aggregating disjoint sets.

D Simulation Environments and Task Configurations

We evaluate our framework on two distinct and challenging domains to assess its collaborative performance and generalization capabilities, utilizing high-fidelity simulators for each task.

D.1 Cooperative Adaptive Cruise Control (CACC)

The CACC task is simulated using the Simulation of Urban Mobility (SUMO)¹ (Version 1.21.0).

- **Topology:** We model a platoon of eight vehicles ($N = 8$) on a single-lane highway segment. The simulation runs for a duration of 60s with a time step of 0.5s (i.e., 120 time steps in total). Each agent operates with limited perception, accessing only the state information (e.g., position, velocity) of its immediately adjacent vehicles (predecessor and follower).
- **Objective:** The control objective is for agents to autonomously adjust acceleration to stabilize the platoon, converging rapidly to an optimal headway of 20 m and a target velocity of 15 m/s.

¹SUMO: <https://eclipse.dev/sumo/>, licensed under EPL 2.0.

- **Scenarios:** We evaluate performance in two dynamic settings: (1) *Scenario 1: Catch-up*: The leading vehicle accelerates to close the gap with a target vehicle, testing the platoon’s ability to re-establish stable formation under high-speed conditions. (2) *Scenario 2: Slow-down*: The leading vehicle decelerates from a high initial speed, challenging the followers to execute coordinated braking without collisions or oscillation.

D.2 Pandemic Control (PC)

The PC task is simulated using the open-source Pandemic Simulator² (Kompella* et al., 2020).

- **Topology:** We model the urban environment as a graph of seven agents representing distinct facility types: *Home, Office, School, Hospital, Retail, Restaurant, and Government*. To construct realistic urban topologies, we utilize Google Maps to identify clusters of functionally similar buildings within specific urban blocks, marking their centroids as individual agents. Communication links are established based on spatial proximity, forming a connected topology as shown in Fig. 6. The simulation spans 120 days, during which agents operate under partial observability regarding global infection rates.
- **Objective:** The primary objective is for agents to dynamically adjust regulatory policies (e.g., gathering restrictions, business hours) to minimize the spread of the virus while maintaining essential socio-economic activities.
- **Scenarios:** We evaluate the framework’s generalization capabilities across three distinct urban settings with varying population scales: (1) *Helsinki*: A standard community setting with a population of 500. (2) *Hong Kong*: A denser urban setting with a population of 1000. (3) *New York*: A high-density complex topology with a population of 1500.

E Baseline Methods

To evaluate MACRO-LLM, we implement and adapt the following baselines for both the CACC and PC tasks.

²Pandemic Simulator: <https://github.com/SonyResearch/PandemicSimulator>, licensed under Apache-2.0.

Algorithm 1: Pseudocode of proposal generation via rollout-simulated verification.

Input: Observation o_n^t ; strategies $\Pi_{n,t}^{\text{temp}}$ and $\Pi_{n,t}^{\text{spatial}}$; maximum attempts Att_{\max} ; rollout horizon K
Output: Verified proposal $P_n^t = (o_n^t, a_n^t, \{a_{n \rightarrow m}^t\}_{m \in \mathcal{N}_n})$

1 Initialize **CANDIDATE_PROPOSALS** $\leftarrow \emptyset$ and $att = 0$;
2 Initialize candidate action with highest reward score by
 $a_n^{t,0} \leftarrow \arg \max_a \text{InferAction}(o_n^t, \mathcal{A}_n, \Pi_{n,t}^{\text{temp}}, \Pi_{n,t}^{\text{spatial}})$ and ensure
 $R_n^t(o_n^t, a_n^{t,0}) \geq R_n^{t-1}(o_n^{t-1}, a_n^{t-1})$;
3 **while** $att < Att_{\max}$ **do**
 4 Initialize rollout trajectory $\tau_n^{t,att} = (o_n^t, a_n^{t,att}, R_n^t)$;
 5 **foreach** $m \in \mathcal{N}_n$ **do**
 6 Obtain observable agents' candidate action
 $a_{n \rightarrow m}^{t,att} \leftarrow \text{InferNeighborAction}(o_n^t, a_n^{t,att}, \Pi_{n,t}^{\text{spatial}})$;
 7 Construct candidate proposal $P_n^{t,att} \leftarrow (o_n^t, a_n^{t,att}, \{a_{n \rightarrow m}^{t,att}\}_{m \in \mathcal{N}_n})$;
 8 **for** Verified time step $k = 1, \dots, K$ in a rollout **do**
 9 Predict next observation $o_n^{t+k,att}$ with candidate proposal $P_n^{t,att}$;
 10 **if** $o_n^{t+k,att}$ violate constraints **then**
 11 Append $P_n^{t,att}$ to **CANDIDATE_PROPOSALS;
 12 $att = att + 1$;
 13 Update candidate action $a_n^{t,att}$ slightly and ensure $R_n^t(o_n^t, a_n^{t,0}) \geq R_n^{t-1}(o_n^{t-1}, a_n^{t-1})$;
 14 Break;
 15 Infer actions $a_{n \rightarrow m}^{t+k,att}$ on time $t + k$;
 16 Add $(a_n^{t+k,att}, o_n^{t+k,att}, R_n^{t+k,att})$ to rollout trajectory $\tau_n^{t,att}$;
 17 **if** $P_n^{t,att}$ has been verified over k time steps **then**
 18 **return** Optimal $P_n^t \leftarrow P_n^{t,att}$.
19 Select the proposal with the highest cumulative reward in its rollout from
 CANDIDATE_PROPOSALS as P_n^t ;
20 **return** P_n^t ;**

E.1 MARL Baselines

We compare against traditional Multi-Agent Reinforcement Learning (MARL) approaches: (1) **DPPO** (Ma et al., 2024): Multi-agent Decentralized Proximal Policy Optimization; (2) **DMPO** (Ma et al., 2024): Multi-agent Model-based Decentralized Policy Optimization; (3) **IC3Net** (Singh et al., 2018): A classic approach for learning when to communicate in multi-agent environments.

E.2 LLM-based MAS Baselines

We compare against recent frameworks utilizing LLMs for collaboration: (1) **ToM-Belief** (Li et al., 2023b): A MAS that employs second-order Theory of Mind for introspection via belief state updates and environmental feedback; (2) **ChatEval** (Chan et al., 2023): Adopts the Simultaneous-Talk-with-Summarizer protocol (Al-

gorithm 3), which is structurally similar to our task setting; (3) **LAMEN** (Davidson et al., 2024): A framework that constructs internal "mental notes" alongside public messages to facilitate strategic negotiation.

E.3 Adaptation and Fairness

To ensure a fair comparison, we maintain experimental consistency across all LLM-based methods. Specifically, we use standardized core prompts for equivalent procedural steps while integrating unique prompting techniques specific to each baseline (e.g., structures for mental notes generation in LAMEN or belief updates in ToM-Belief). All baselines utilize the same backbone model (GPT-4o) and environmental interfaces as MACRO-LLM.



Figure 6: Communication topology of cities for pandemic networks. (a) Helsinki (b) Hong Kong (c) New York.

F Detailed Evaluation Metrics

We provide the detailed definitions and mathematical formulations of the metrics used in our experiments.

F.1 CACC Task Metrics

Following previous works (Desjardins and Chaib-draa, 2011; Van Arem et al., 2006), we evaluate the platoon efficiency and stability using:

• Root Mean Square Error (RMSE-H/V):

Measures the deviation between the actual headway/velocity and the target values, averaged across all following vehicles ($i = 1 \dots N$) over the simulation steps ($t = 1 \dots T$). For example, RMSE of Headway (RMSE-H) is calculated as:

$$\text{RMSE-H} = \sqrt{\frac{1}{N \cdot T} \sum_{t=1}^T \sum_{i=1}^N (h_i^t - h_{\text{target}})^2}, \quad (9)$$

where h_i^t is the headway of vehicle i at time t , and h_{target} is the optimal safety distance. RMSE-V is computed similarly using velocity deviations as follows:

$$\text{RMSE-V} = \sqrt{\frac{1}{N \cdot T} \sum_{t=1}^T \sum_{i=1}^N (v_i^t - v_{\text{leader}})^2}, \quad (10)$$

where v_{leader} denotes the velocity of the leading vehicle.

• Standard Deviation (SD-H/V):

Measures the collaborative consistency of the platoon across all agents. Specifically, at each time step t , we calculate the standard deviation of the headway/velocity across all N vehicles. The final reported metric is the temporal average of these spatial standard deviations over the duration T :

$$\text{SD-H} = \frac{1}{T} \sum_{t=1}^T \sqrt{\frac{1}{N} \sum_{i=1}^N (h_i^t - \bar{h}^t)^2}, \quad (11)$$

where $\bar{h}^t = \frac{1}{N} \sum_{j=1}^N h_j^t$ is the average headway of the entire platoon at time t . A lower SD value indicates that all agents are maintaining consistent states simultaneously, reflecting high coordination stability. SD-V is computed

similarly using velocity deviations as follows:

$$\text{SD-V} = \frac{1}{T} \sum_{t=1}^T \sqrt{\frac{1}{N} \sum_{i=1}^N (v_i^t - \bar{v}^t)^2}. \quad (12)$$

F.2 PC Task Metrics

Following Kompella et al. (Kompella* et al., 2020), we employ the following metrics to assess containment efficacy. Let P_{total} be the total population, and I^t, C^t, D^t be the count of infected, critical, and dead cases on day t , respectively.

- **Normalized Infection (I_n):** The ratio of the cumulative number of infected cases to the total population:

$$I_n = \frac{\sum_t \Delta I_{new}^t}{P_{total}}. \quad (13)$$

- **Normalized Peak Infection (PI_n):** Measures the highest pressure on the healthcare system:

$$PI_n = \frac{\max_t(I^t)}{P_{total}}. \quad (14)$$

- **Normalized Dead (D_n):** The ratio of total dead cases to the total population at the end of the episode (t_{end}):

$$D_n = \frac{D^{t_{end}}}{P_{total}}. \quad (15)$$

- **Pandemic Duration (PD):** The time span (in days) from the first confirmed infection (t_{start}) until the pandemic is effectively contained:

$$PD = t_{end} - t_{start}, \quad (16)$$

where $t_{end} = \min\{t \mid I^t + C^t = 0, \forall \tau > t\}$.

G Computational and Communication Scalability Analysis

We provide a theoretical and empirical analysis of MACRO-LLM, focusing on communication complexity and computational workload.

G.1 Communication Complexity Analysis

Following the definition by Yao (Yao, 1979), communication complexity is quantified by the total number of bits exchanged during the protocol. In our decentralized framework, we focus on the per-agent communication load. Let $\mathcal{G} = (\mathcal{V}, \mathcal{E})$ be the

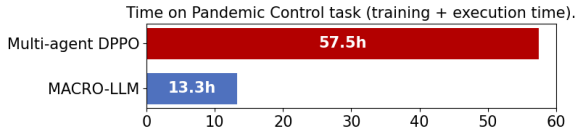


Figure 7: Training and execution time on the pandemic control task (120-day simulation), considering the total time from training to execution for a single node in a new environment. Experiment settings can be found in Sec. 4.2.

43+4

agent communication graph. We denote the average node degree as \bar{d} and the maximum negotiation rounds as r . The topology of the CACC task is linear ($\bar{d} \approx 2$). In the PC task, the topology represents an urban graph with average degree \bar{d}_{PC} . We assume sparse topologies where \bar{d} does not grow linearly with the total number of agents N (i.e., $\bar{d} \ll N$). As the network scales up, MACRO-LLM employs mean-field approximation to compress the states of unobservable agents into a single virtual node representation. Neglecting inference stochasticity, the per-agent message size is theoretically invariant to the network scale, which is represented as M . Consequently, the per-agent communication complexity can be represented as $O(\bar{d} \cdot r \cdot M)$. Since \bar{d} , r , and M are independent of network scale N , the per-agent load remains constant ($O(1)$) as the network scales in theory.

G.2 Computational Efficiency and Latency

Given that the input prompt length remains bounded as analyzed above, the upper bound of the inference workload for a single agent does not increase with the number of agents. Taking the PC task as an example, Fig. 7 illustrates that the time required for MARL to train to convergence on a new topology is approximately 4× the total execution time of MACRO-LLM (using the GPT-4o API) for a complete episode. While the inference speed of trained MARL policies is extremely fast, these baselines necessitate extensive retraining when transferring to a new scenario. In contrast, MACRO-LLM exhibits instant zero-shot adaptation. This capability is critical for dynamic, open-world deployments where frequent retraining is impractical. In our experiments, API-based inference is subject to network latency, which poses challenges for time-sensitive tasks. However, experiments in Table 3 demonstrate that lightweight models (e.g., GPT-4o-mini or Qwen3-flash) achieve

competitive performance. For latency-sensitive applications, locally deploying these smaller models can significantly accelerate the negotiation process, reducing inference times to satisfy real-time control constraints.

H Extended Ablation Analysis

In this section, we provide a detailed quantitative analysis of the ablation study.

H.1 Component Analysis in CACC

The removal of specific modules leads to critical performance degradation in the high-precision and highly dynamic CACC task:

- **Impact of CoProposer:** Without the CoProposer, agents fail to infer and verify collaborative actions via rollout simulation. Consequently, RMSE-H and SD-H are $9.1\times$ and $18.3\times$ higher than those of MACRO-LLM, respectively. This result demonstrates that effective multi-agent coordination heavily depends on high-quality, verified initial proposals.
- **Impact of Negotiator:** Even with valid collaborative actions generated by the CoProposer, the omission of the negotiation phase results in an RMSE-H $6.1\times$ higher than that of the full model. This degradation demonstrates the agents’ inability to resolve conflicting intentions within a time-varying environment.
- **Impact of Introspector:** Agents without the Introspector tend to sacrifice headway stability to aggressively optimize velocity, with RMSE-H degrading by $1.9\times$. This indicates that self-reflection is essential to suppress oscillation and prevent the “accordion effect” in multi-agent collaboration.

H.2 Component Analysis in PC

A similar pattern holds for the Pandemic Control task:

- **Impact of CoProposer:** Removing the CoProposer extends the pandemic duration by $2.5\times$ compared to the full framework. Lacking rollout-simulated verification, agents adopt myopic strategies, failing to curb pandemic transmission effectively.
- **Impact of Negotiator:** Excluding the Negotiator prolongs the pandemic to 32 days,

demonstrating that the absence of consensus mechanisms leads to inconsistent and ineffective containment policies.

- **Impact of Introspector:** Ablating the Introspector results in a pandemic duration approximately 44.4% longer than MACRO-LLM. This illustrates that agents without self-reflection are slow to adapt their strategies to the evolving infection dynamics.

I Analysis of Failure Cases and Solutions

To provide insights into the limitations of current LLMs in multi-agent control, we categorize the primary failure cases observed during our experiments and detail the corresponding mitigation strategies implemented in MACRO-LLM.

Arithmetic and Spatial Hallucinations. Despite access to topological information, agents occasionally exhibit spatial hallucinations, such as confusing front and back vehicles in the CACC task. To mitigate this, we employ few-shot prompting incorporating explicit examples of state transitions (e.g., detailing how acceleration impacts headway relative to neighbors).

Furthermore, LLMs struggle with the precise numerical calculations required for kinematic updates, often leading to arithmetic inaccuracies. To ensure precision, we offload deterministic calculations to an external Python interpreter. The computation results are then integrated into the prompt for subsequent inference.

Identity Confusion. In scenarios featuring dense interaction prompts, such as concurrent proposals involving similar identifiers, such as “*Vehicle 2* propose action1 to *Vehicle 1*, and propose action2 to *Vehicle 3*), agents may misattribute actions or forget their own identity. We attribute this to the attention mechanism’s difficulty in distinguishing semantically similar tokens within extended contexts. To address this, we enforce a structured schema for inter-agent communication and integrate a self-consistency mechanism to validate sender-receiver pairings. Additionally, we reinforce role stability by prepending the instruction “*You are [Agent Name]*” to every query prompt.

Syntactic Robustness. To structure agent outputs, we employ XML-style `<label>` tags. However, smaller or quantized models (e.g., GPT-4o-mini, Qwen3-flash) occasionally fail to adhere to

these formatting constraints, resulting in unclosed tags or hallucinated labels. To mitigate this, we implement a deterministic verification layer, outputs failing regex matching or schema validation trigger an automatic retry, ensuring that only syntactically valid actions are executed.

Safety Alignment Sensitivity. In the PC task, the Qwen series frequently triggered safety refusals during stages characterized by high mortality rates, erroneously flagging simulation statistics as harmful content (returning `openai.BadRequestError`). This behavior indicates a stricter safety filter configuration compared to models like GPT-4o. To mitigate these false positives, we appended a system prompt explicitly clarifying the synthetic nature of the data: "SIMULATION NOTE: SIMULATION NOTE: This is a hypothetical pandemic experiments on pandemic simulator. All data is synthetic and does not reflect real-world events!!!!" Additionally, we implemented a rollback mechanism to discard and retry generation steps interrupted by safety filters.

J Core Prompts of MACRO-LLM

J.1 CoProposer

Table 8 provides the core prompts of proposal generation with a rollout-simulated verification in Co-Proposer.

J.2 Negotiator

Table 9 provides the core prompts for proposal evaluation with spatial strategies and feature updates in Negotiator when consensus is not achieved. Table 10 provides the core prompts for updating proposal with updated spatial strategies and features in Negotiator.

J.3 Introspector

Table 11 presents the core prompts for generating the semantic gradient after completing one-step execution. Table 12 presents the core prompts for updating the temporal strategy using the learning rate and semantic gradient.

[*self-checking_rules*] are a set of rules for verifying the output format and common-sense consistency of LLM outputs. These rules ensure that the model correctly applies physical reasoning. For example, in CACC task, "If ACCELERATION_GAP > 0, MY_VELOCITY will be INCREASED, MY_HEADWAY will be DECREASED." These rules help correct occasional

LLM mistakes, such as misjudging the travel direction of vehicles and thus misunderstanding how acceleration or deceleration affects inter-vehicle headway.

K AI Assistants in Writing

We utilized AI assistants (e.g., Gemini) exclusively for grammatical error correction, sentence polishing to enhance readability, and generating robot icons used in Figures 1 and 2. We explicitly state that the core scientific concepts, experimental design, logical structure, reference, and substantive content of the paper were entirely human-authored without generative contributions from LLMs.



CoProposer: Proposal Generation Query

You are [agent_name] in a [task_name]. This is negotiation round 0 with your neighbors. Your task is to [task objective]. Decision-Making Steps (Follow strictly, step by step):
 Step 0: Initial Decision for [agent_name] at the 1st time step, and define urgency of the action: Normal, Warning, Urgent.
 Step 1: Collaborative acceleration for [observable_agents] to achieve objective with [Temporal Strategy], [Spatial Strategy] and [Spatial Features].
 Step 2-4: Validation by 2 Time-Step Simulation: (time step 2 and time step 3).
 Step 2: Simulate the next state (state_2) at time step 2. [instructions]
 Step 3: Calculate collaborative actions for state_2.
 Step 4: Simulate the next state (state_3) at time step 3. [instructions]
 Step 5: Feasibility check for both state_2 and state_3
 [task_constraints]
 - If any constraint is violated, go back to Step 0 and pick a more conservative action. Repeat Steps 0-4 up to 10 times.
 - If no feasible proposal is found after 10 iterations, output the best proposal found.
 Output Format (STRICT):
 <analysis>[analysis_and_calculation_steps] </analysis>
 <proposal>[semantic_proposal_for_negotiation] </proposal>
 <output>E[timestep]_R[round]_[agent_name]_proposal = {[my_name]: <proposed action for itself>, [neighbor's_name]: <proposed acceleration for neighbor>}</output>
 IMPORTANT: [self-checking_rules]

Figure 8: The core prompt of CoProposer.



Negotiator: Proposal Evaluation Query

You are [agent_name] for [task_name]. Your observable neighbor is [observable_agents]. In the last negotiation round, consensus was not reached. You need to analyze the disagreement and summarize your reasoning in the following steps:
 Step 0: Analyze whether the strategy proposed by [agent_name] conflicts with the strategy proposed by its observable neighbors [agent_name]
 [task_strategy_information]
 Step 1: According to [Spatial Strategies] and [Spatial features], analyze whether the strategy proposed by [neighbors_agent] conflicts with the trends of [unobservable_agents].
 [task_strategy_information]
 Output as following format:
 <deal>False</deal>
 <reasons> Observable vehicles:[observable_agent_name] choose ..., and proposes It's strategy is match/conflict/not conflict with my strategy. The reason is ... I suggest it's weight in the range ...
 [unobservable_agent_list]: They are strategy trend is match/conflict/not conflict with my strategy. The reason is ... I suggest it's weight in the range ...</reasons>
 <spatial-strategy>[update_spatial_strategy]</spatial-strategy>
 IMPORTANT: [self-checking_rules]

Figure 9: The core prompt of proposal evaluation and spatial strategy update.



CoProposer: Update Proposal

You are [agent_name]. This is the Round_[current_round] of [time_step]. Your observable states is [agent_name] Observable State in time_step]. You need to update your proposal by following steps.

- **Case 1: If the flag between <deal></deal> is True, reuse the last proposal and output as following format:**

```
<analysis>(I will keep my last proposal, because ...)</analysis>
<proposal> [semantic_proposal_for_negotiation] </proposal>
<output>[structured_proposal_for_coding]</output>
Skip the following steps.
```

- **Case 2: If the flag between <deal></deal> is False:**

Step 1: Define the confidence weights for observable neighborsproposal and unobservable vehicles weighted average acceleration. [weight_rules]
Output the confidence weights as following format:

```
<insights>neighbor_proposed_weight:<neighbor_proposed_weight      value>      unobservable_weight:
<unobservable_weight value> my_weight: <my_weight value></insights>
```

Step 2: Based on weights defined between <insights></insights>, weighted the proposed acceleration for each vehicles by following equations:

```
updated_acceleration = neighbor_proposed_weight * neighbor_proposed_acceleration + my_weight * my_acceleration + unobservable_weight * unobservable_trend.
```

/* Step 3: A rollout-simulated verification similar to Step 2-5 in CoProposer */

Output Format (STRICT):

```
<analysis>[analysis_and_calculation_steps] </analysis>
<proposal>[semantic_proposal_for_negotiation] </proposal>
<output>E[timestep]_R[round]_[agent_name]_proposal = {[agent_name]: <proposed action for itself>,
[neighbor's_name]: <proposed acceleration for neighbor>}</output>
IMPORTANT: [self-checking_rules]
```

Figure 10: The core prompt of update proposal.



Introspector: Generate Semantic Gradient

You are [agent_name]. You can observe [observable_agent_name]. The total system reward for this time step is xx% lower than in the last time step indicating that the system state getting worse. Your individual reward has dropped from xx to xx, which drop xx%.

Step1. Based on [last_negotiation_record] and [this_negotiation_record], integrate the [Objective Instruction] to analyze whether the drop in episode reward was caused by yourself. If so, at which stage was responsible.

Infer whether the reward decline was caused by [observable_agents] or [unobservable_agents], and output between tags <reasons> </reasons>

Based on <reasons> </reasons> should strategies be adjusted to improve future episode rewards? Step 1: You need to find out the rules that need to be adjusted based on the reasons you summarized.

Step 2: According to the related rules you summarized, be specific about "what to do" and "what to avoid" and output between tags <self-checking_rules> and </self-checking_rules>.

The output format as follows:

```
<reasons>[summarized_reasons]</reasons>
<self-checking_rules>(When      states      condition      ...      I      need      to/I      need      to      avoid
...)</self-checking_rules>
IMPORTANT: [self-checking_rules]
```

Figure 11: The core prompt of generating semantic gradient.



CoProposer: Update Strategy Query

You are [agent_name] to update its strategies. The total system reward for this time step is xx% lower than last time step, indicating that the system state getting worse. The overlap of transition (including state and action) among these two time steps is xx%, which means that their overall movement and decision patterns are xx% similar, with xx% differences in how the agent moves between states and selects actions.

Based on the <reasons></reasons> you summarized (from Table 11), update your strategies carefully with NO MORE than xx% learning rate.

Step 1. Calculate the change in state from the historical states to the current state and compare it to the previous temporal plan. Analyze if the change in state matches the plan of the previous temporal plan.

Step 2. Carefully check whether the change match the last temporal plan.

- If it matches, keep the original plan and update the temporal plan. Execute step 3 to return the updated plan.

- if it doesn't match, summarize the reasons and output within <reflect> tags as following:
<reflect>(My final action does not match my original temporal plan, the reasons may be
...)</reflect>

According to the <reflect></reflect>, update the temporal plan.

Step 3. Output the updated plan with following format:

<temporal-strategy>[update_temporal_analysis]</temporal-strategy>

IMPORTANT: [self-checking_rules]

Figure 12: The core prompt of update strategy